Experimental homogenized elastic properties of computer-generated 3D-printed random porous material

O. Zerhouni, M G Tarantino, K. Danas

Experimental homogenized elastic properties of computer-generated 3D-printed random porous material

O. Zerhouni[a], M. G. Tarantino[a], K. Danas,[a,*]

[a] *LMS, C.N.R.S., École Polytechnique, 91128 Palaiseau, France*

Abstract

The present study introduces a methodology that allows for the combination of 3D-printing, experimental testing, numerical and analytical analysis of random porous materials with controlled homogenized elastic properties. These microstructures are computer-generated based on a random sequential addition algorithm with statistically controlled morphological properties such as volume fraction, shape and size of voids as well as isotropic distribution of their centers. We first focus on porous material containing single-size (monodisperse) spherical voids. The porous specimens are fabricated by 3D printing with polymer jet technology and then microstructures are aposteriori investigated by optical microscopy and SEM. The influence of the 3D printing process parameters is also experimentally assessed. An experimental protocol is developed in order to obtain the effective elastic properties of the porous specimens.

Keywords: Additive manufacturing, Hashin-Shtrikman bounds, Random Sequential Adsorption, Random composites, Homogenization, Porous Materials, Effective properties

1. Introduction

Porous materials are present in nature (e.g., rocks and geomaterials) but can also be designed to allow for controlled stiffness of lightweight structures. Recent development of additive manufacturing processes has led to new methods for generating complex microstructures that can achieve high-performance lightweight properties. The porous materials fabricated by 3D printing find applications in high-stiffness lightweight structures (Zok et al., 2004; Berger et al., 2017), acoustic and vibration dampers (Göransson, 2006; Banhart et al., 1996; Ma et al., 2013), impact energy absorbers (Davies and Zhen, 1983), high electric capacitors (Wang et al., 2008) and filtration (Alderson et al., 2000) among others.

In this study, we are interested in transferring theoretical and virtual microstructures that are very close to the Hashin-Shtrikman bounds numerically to fabrication and experimental testing.IThis aims at introducing a methodology that allows to combine 3D printing, experimental testing, numerical and analytical

*Corresponding author.

Email addresses: `othmane.zerhouni@polytechnique.edu` (O. Zerhouni), `maria-gabriella.tarantino@polytechnique.edu` (M. G. Tarantino), `konstantinos.danas@polytechnique.edu` (K. Danas,)

modeling in order to create random close-cell porous materials with effective elastic properties that approach the Hashin-Shtrikman bounds. In this study, we focus on isotropic random microstructures consisting of single sized (i.e. monodisperse) spherical voids embedded in a homogeneous solid matrix. Those microstructures are shown to have almost identical effective elastic properties with multiple size (i.e. polydisperse) microstructures for volume fractions up to 30%.

2. Generation of random isotropic porous materials

2.1. RSA generation of isotropic random spherical inclusions

We use the random sequential adsorption algorithm (Rintoul and Torquato, 1997; Segurado and Llorca, 2002; Lopez-Pamies et al., 2013) to construct the virtual microstructures of the present study. We use as input parameters the porosity c and the number of pores N to create spherical voids that are distributed randomly in a cubic cell of volume L^3. In thiss study, we set the minimal distance between two voids at 150μm. We note in passing that this distance can be further reduced to allow larger volume fractions. However, a minimum spacing between non connected voids is needed so that they can be properly manufactured by our 3D printer. For illustration purposes, Fig. 1 shows three such RVEs comprising monodisperse spherical voids of increasing porosity $c = \{10, 20, 30\}\%$.

2.2. RVE size and related boundary conditions

The choice of N is made in order to have the ratio D/L, with D and L denoting the diameter of the voids and the edge length of the cubic cell, large enough to obtain numerical effective properties that are independent on boundary conditions.(Suquet, 1987; Kanit et al., 2003) These are computed from the average stress and strain fields using the overall constitutive equation (Hill, 1963)

$$\langle \boldsymbol{\sigma}(\mathbf{x}) \rangle = \widetilde{\mathbb{C}} : \langle \boldsymbol{\varepsilon}(\mathbf{x}) \rangle \tag{1}$$

where $\langle \boldsymbol{\varepsilon}(\mathbf{x}) \rangle = \overline{\boldsymbol{\varepsilon}}$ is the macroscopic imposed strain, $\widetilde{\mathbb{C}}$ denotes the overall stiffness tensor and the notation $\langle . \rangle$ is used to denotes volume averages. In practice, adopting Voigt notation, each column of the stiffness tensor $\widetilde{\mathbb{C}}$ is computed by imposing a strain field in a specific direction(Kanit et al., 2003). For example, imposing the overall strain field $\overline{\boldsymbol{\varepsilon}} \equiv (\overline{\varepsilon}_{11}, 0, 0, 0, 0, 0)$, we obtain six linear relations: $\widetilde{C}_{kl11} = \overline{\sigma}_{kl}/\overline{\varepsilon}_{11}$ with $kl = 11, 22, 33, 12, 23, 31$. The computation of all six columns of $\tilde{\mathbb{C}}$ is done by application of six independent loads $\overline{\boldsymbol{\varepsilon}}$ as described in (Kanit et al., 2003).

The matrix phase is modeled by an isotropic linear elastic constitutive behavior with Young's Modulus $E = 1.4$ GPa and Poisson's ratio $\nu = 0.42$ corresponding to those of the matrix phase used in the 3D-rinting. Results of the experiments on microstructures from 1% to 30% porosity are shown in Fig. 2.

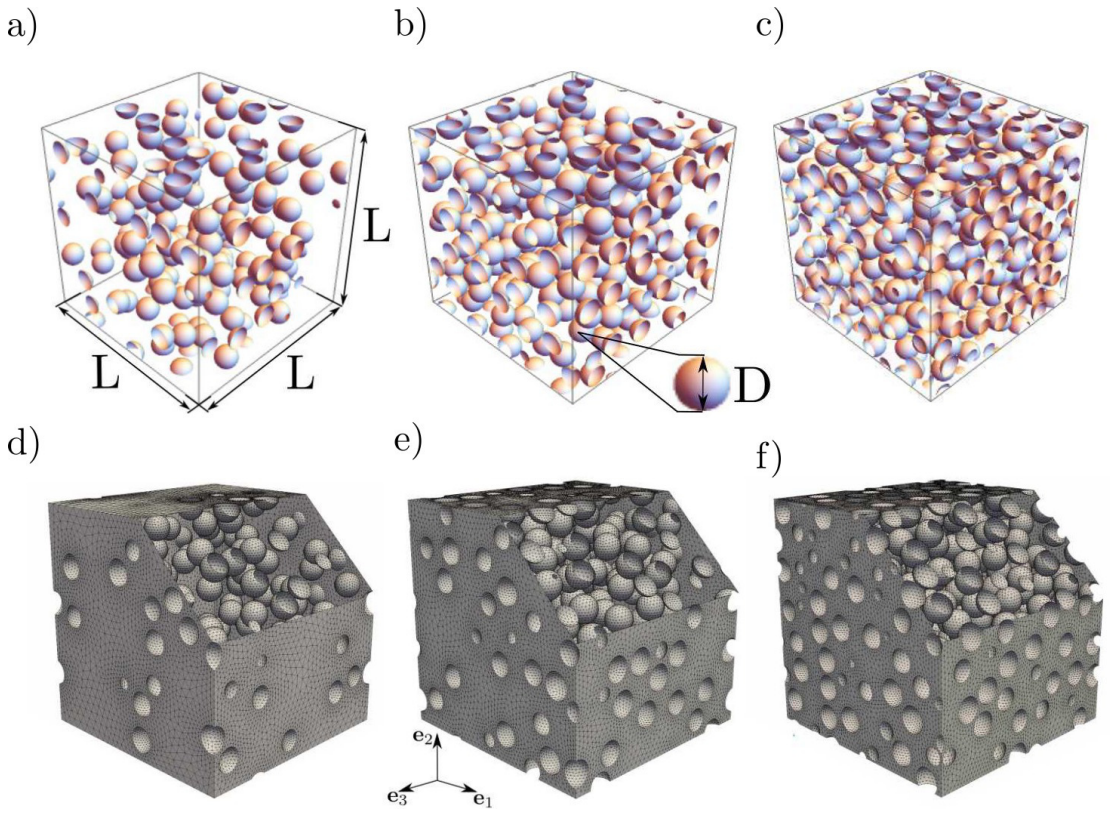

Figure 1: RVEs of unit volume L^3 with N randomly distributed spherical particles of monodisperse sizes for a total porosity (a) $c = 10\%$ and $N = 160$, (b) $c = 20\%$ and $N = 275$, (c) $c = 30\%$ and $N = 400$. (d-f) Representative meshes corresponding to the undeformed configuration of the representative cubic cells.

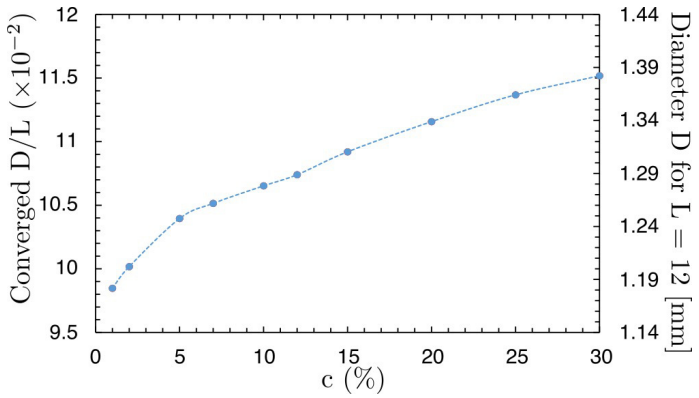

Figure 2: (Right axis) Converged pore to cube size ratio D/L and (left axis) pore diameter (in mm) for a cube side length $L = 12$mm as a function of the porosity c.

3. Additive manufacturing and experimental methods

In order to construct the virtual geometry of the porous samples, we adopt the protocol shown in Fig. 3. We first assemble length-wise five representative cubic RVE cells of length $L = 12$mm in order to build the reduced uniform section of the test specimens. The latter is enclosed between the heads of the sample which, in turn, have a solid section thus allowing us to mount the specimen onto the uniaxial machine.

We use commercial software NETGEN to transform the 3D virtual model of our test specimens into a stereolitography format (i.e. STL) to 3D-printing. We assess the dimensional accuracy of the 3D-printed porous microstructures by use of an optical microscope. Overall, Fig. 4 reveals that pores with circular section can be manufactured with very good dimensional accuracy within the range of size required by our numerical RVE analysis for $L = 12$mm. Finally, it is worth mentioning that no additional micron-size porosity has been observed in the matrix phase as a result of the printing process.

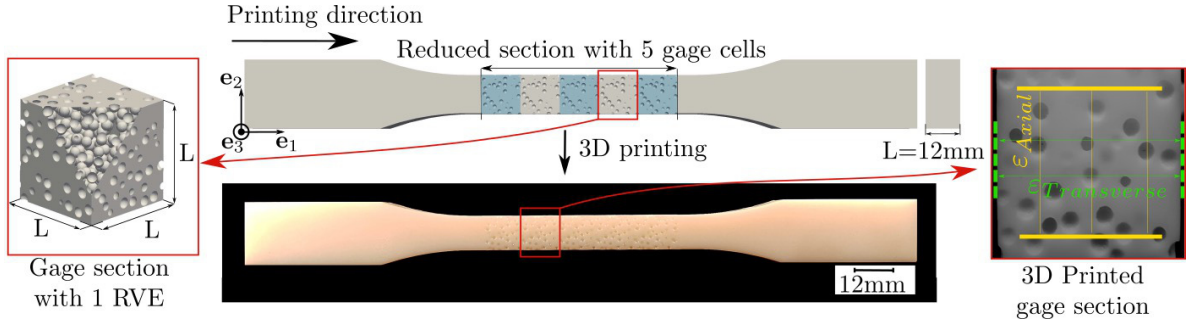

Figure 3: (Top) Virtual testing sample generated by assembling length-wise 5 cubic porous RVEs and by adding gripping heads of solid material. (Left) A zoom of the RVE which defines our gage section. (Bottom) 3D printed testing sample after cleaning support material from open pores and boundary surface. (Right) A zoom of the 3D printed RVE showing the size of the actual axial and transverse gage sections in the experiment.

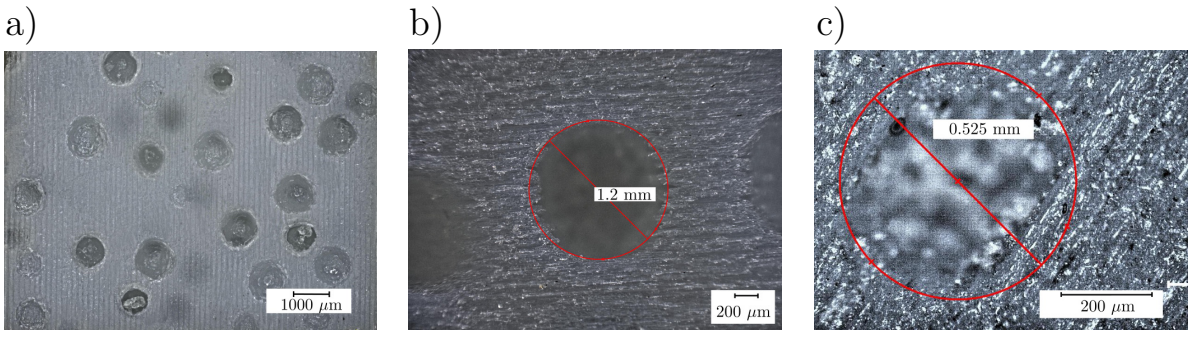

Figure 4: Optical image showing a cross-section of the macroscopic 3D printed specimen with the spherical pores for the assessment the printing accuracy. Observations of representative 3D printed spherical voids of diameter (b) $D \sim 1.2$mm and (c) $D \sim 0.500$mm. A fairly good printing accuracy is observed in both cases.

The main aim of the experiments is then the measurement of the effective Young's modulus and Poisson's ratio of the 3D-printed random porous microstructures. Following the experimental methodology presented in Hossain et al. (2012), we measure the elastic parameters by means of a multi-step relaxation testing, as shown in Fig. 5a, to overcome any effect of the viscosity in the material. To assess reproducibility of the data, we use four specimens for each test.

The effective Young's modulus, $\widetilde{E}$ (or E_m for the pure polymer), is evaluated as the slope of the line connecting the equilibrium (fully relaxed) stress points in the nominal stress-strain curve as shown in Fig. 5b and the calculation of the Poisson's ratio is found by the slope of transverse strain-axial strain curve.

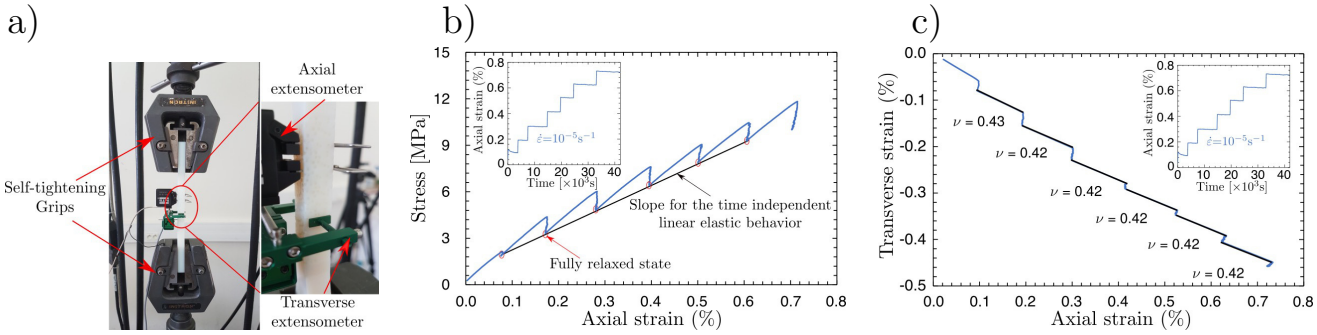

Figure 5: Overall applied strain rate $\dot{\varepsilon} = 10^{-5}\text{s}^{-1}$: (a) Stress-Strain curves obtained during multi-step relaxation steps. The Young's modulus is obtained by the slope of the curve that connects the fully relaxed stress states excluding the first point. (b) Axial versus transverse strain curve during the mult-step relaxation test. Slopes during loading are found to be fairly independent of the level of the axial strain.

The experimental results for the matrix and support material following this procedure provide experimental evidence that the matrix material (VeroWhite) is statistically homogeneous and exhibits an elastically isotropic behavior with a Young's modulus $E_m = 1400 \pm 120$MPa and a Poisson's ratio of $\nu_m = 0.42 \pm 0.02$. These moduli correspond to a bulk modulus of $\kappa_m = 2920$MPa and a shear modulus of $\mu_m = 493$MPa. In turn, it indicates that the support material, used by 3D printer to fabricate the spherical pores, has negligible elastic properties when compared with those of the matrix material (VerowhitePlus) thereby having no effect on the effective porous material response.

3.1. Results and Discussion

For isotropic porous materials, the Hashin-Shtrikman bounds (Hashin and Shtrikman, 1963; Willis, 1977) are given by

$$\widetilde{\kappa}_{HS} = \frac{4(1-c)\mu_m\kappa_m}{4\mu_m + 3c\,\kappa_m} \quad , \quad \widetilde{\mu}_{HS} = \frac{(1-c)(8\mu_m + 9\kappa_m)\mu_m}{4\mu_m(2+3c) + 3\kappa_m(3+2c)} \tag{2}$$

where κ_m and μ_m denote the bulk and shear moduli of the matrix phase, respectively and c the volume fraction of the inclusion phase or porosity in the present context. The corresponding effective Young's

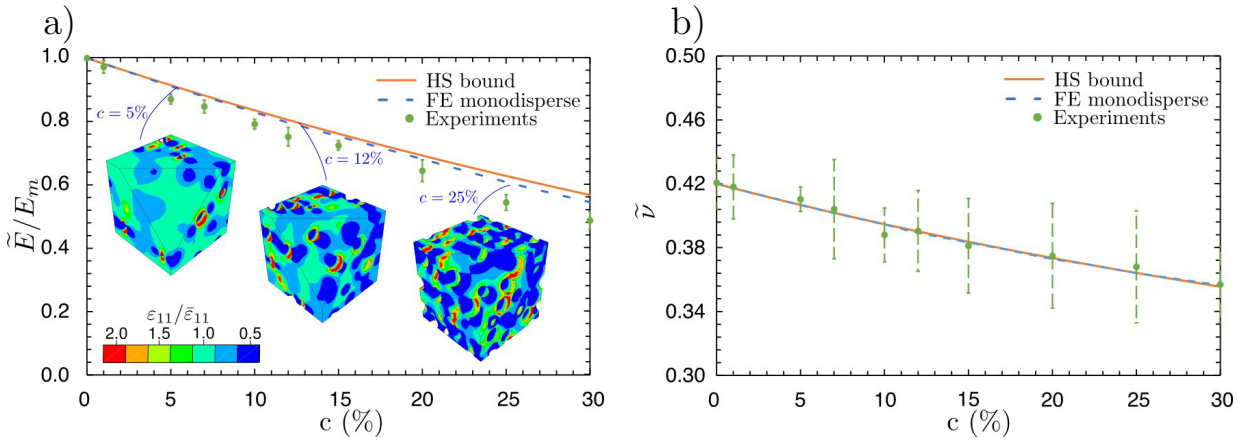

Figure 6: Normalized with the matrix properties effective (a) Young's modulus $\widetilde{E}/E_m$, (b) Poisson's ratio $\widetilde{\nu}$ as a function of the porosity c. Comparison between the analytical HS bounds, FE monodisperse numerical estimates and experimental results.

modulus, $\widetilde{E}$ and Poisson's ratio, $\widetilde{\nu}$, are readily obtained by $\widetilde{E} = 9\widetilde{\kappa}\widetilde{\mu}/(3\widetilde{\kappa} + \widetilde{\mu})$ and $\widetilde{\nu} = (3\widetilde{\kappa} - 2\widetilde{\mu})/(6\widetilde{\kappa} + 2\widetilde{\mu})$, respectively. Figure 6 shows the effective (a) Young's modulus $\widetilde{E}$, (b) Poisson's ratio $\widetilde{\nu}$, (c) bulk modulus $\widetilde{\kappa}$ and (d) shear modulus $\widetilde{\mu}$ as a function of the porosity c. We observe that the experimental results for the directly measured $\widetilde{E}$ are in very good agreement with the numerical FE results, which almost overlap with the HS bounds even for porosities as large as $c = 30\%$. The maximum deviation of the experimental $\widetilde{E}$ from the HS bound is 8% when $c = 30\%$. Differences between similar measures can be due either to the ageing of the polymeric material during 3D printing or to experimental uncertainty. Similar to $\widetilde{E}$, both the $\widetilde{\kappa}$ and $\widetilde{\mu}$ obtained by the experiments are very close to the theoretical HS bounds.

4. Concluding remarks

In this work, we have investigated the influence of some geometrical features of the microstructure on the effective elastic propertiesof random isotropic close-cell porous materials by means of a numerically-aided additive manufacturing procedure. Results show that the size of the pores does not affect the overall experimental elastic properties of the 3D printed material and that strain localization seems to cause the effective properties of the material to depart from the Hashin-Shtrikman bound.

The present study can be extended to larger porosities, at least up to $c = 70\%$ (or relative density $\rho = 1 - c = 0.3$) using polydisperse distributions of particles.

References

Alderson, A., Rasburn, J., Ameer Beg, S., Mullarkey, P.G., Perrie, W., Evans, K.E., 2000. An auxetic filter: a tuneable filter displaying enhanced size selectivity or defouling properties. Industrial Engineering Chemistry Research 39, 654–665.

Banhart, J., Baumeister, J., Weber, M., 1996. Damping properties of aluminium foams. Materials Science and Engineering: A 205, 221 – 228.

Berger, J.B., Wadley, H.N.G., McMeeking, R.M., 2017. Mechanical metamaterials at the theoretical limit of isotropic elastic stiffness. Nature 543, 533 EP –.

Davies, G.J., Zhen, S., 1983. Metallic foams: their production, properties and applications. Journal of Materials Science 18, 1899–1911.

Göransson, P., 2006. Acoustic and vibrational damping in porous solids. Philosophical Transactions of the Royal Society of London A: Mathematical, Physical and Engineering Sciences 364, 89–108.

Hashin, Z., Shtrikman, S., 1963. A variational approach to the theory of the elastic behaviour of multiphase materials. Journal of the Mechanics and Physics of Solids , 127–140.

Hill, R., 1963. Elastic properties of reinforced solids: Some theoretical principles. Journal of the Mechanics and Physics of Solids 11, 357 – 372.

Hossain, M., Vu, D., Steinmann, P., 2012. Experimental study and numerical modelling of vhb 4910 polymer. Computational Materials Science 59, 65–74.

Kanit, T., Forest, S., Galliet, I., Mounoury, V., Jeulin, D., 2003. Determination of the size of the representative volume element for random composites: statistical and numerical approach. International Journal of Solids and Structures 40, 3647 – 3679.

Lopez-Pamies, O., Goudarzi, T., Danas, K., 2013. The nonlinear elastic response of suspensions of rigid inclusions in rubber: Ii—a simple explicit approximation for finite-concentration suspensions. Journal of the Mechanics and Physics of Solids 61, 19 – 37.

Ma, Y., Scarpa, F., Zhang, D., Zhu, B., Chen, L., Hong, J., 2013. A nonlinear auxetic structural vibration damper with metal rubber particles. Smart Materials and Structures 22, 084012.

Rintoul, M., Torquato, S., 1997. Reconstruction of the structure of dispersions. Journal of Colloid and Interface Science 186, 467 – 476.

Segurado, J., Llorca, J., 2002. A numerical approximation to the elastic properties of sphere-reinforced composites. Journal of the Mechanics and Physics of Solids 50.

Suquet, P., 1987. Homogenization Techniques for Composite Media: Lectures Delivered at the CISM International Center for Mechanical Sciences Udine, Italy, July 1–5, 1985. Springer Berlin Heidelberg, Berlin, Heidelberg. pp. 193–230.

Wang, D.W., Li, F., Liu, M., Lu, G., Cheng, H.M., 2008. 3d aperiodic hierarchical porous graphitic carbon material for high rate electrochemical capacitive energy storage. Angewandte Chemie International Edition 47, 373–376.

Willis, J., 1977. Bounds and self-consistent estimates for the overall properties of anisotropic composites. Journal of the Mechanics and Physics of Solids 25, 185 – 202.

Zok, F., Waltner, S., Wei, Z., Rathbun, H., McMeeking, R., Evans, A., 2004. A protocol for characterizing the structural performance of metallic sandwich panels: application to pyramidal truss cores. International Journal of Solids and Structures 41, 6249 – 6271.